Preprints, 10th Conference on Manoeuvring and Control of Marine Craft
August 24-26, 2015. Copenhagen, Denmark

A Virtual Vertical Reference Concept for GNSS/INS Applications at the Sea Surface

Torleiv H. Bryne * **Thor I. Fossen** * **Tor A. Johansen** *

* *Centre for Autonomous Marine Operations and Systems (AMOS), Department of Engineering Cybernetics, Norwegian University of Science and Technology, 7491 Trondheim, Norway (e-mail: torleivh.bryne@itk.ntnu.no, thor.fossen@ntnu.no, tor.arne.johansen@itk.ntnu.no).*

Abstract: Inertial navigation systems (INS) can be used to obtain estimates of the position, velocity and attitude, in a dead-reckoning fashion, for marine vessels. To combat drift, aiding reference systems such as global navigation satellite systems are utilized. However, satellite based positioning systems typically provide less accurate measurements of the vertical position. This paper presents an alternative vertical aiding by introducing a virtual vertical reference concept with respect to uncoupled and loosely coupled GNSS/INS integration, which improves the accuracy of nonlinear observers significantly when applied to strapdown inertial navigation. The estimation performance obtained with the virtual vertical reference concept is compared with the performance obtained with standalone GNSS, and differential corrected GNSS through simulations.

Keywords: Inertial navigation; Navigation systems, Position estimation, Nonlinear observers; Marine systems

1. INTRODUCTION

Estimation of position, velocity and attitude (PVA) is carried out and applied in a variety of technology segments, for instance in consumer electronics, the automotive industry, robotics, and for aerial and marine surface vehicles. Strapdown inertial navigation systems (INS) can be utilized for PVA estimation in all of these segments. An INS is based on inertial measurements, such as rate gyro and specific force measurements provided by an inertial measurement unit (IMU). These measurements are integrated once and twice, respectively, usually using an observer in a dead-reckoning fashion. Over longer time periods the INS estimates are prone to drift due to inertial sensor errors, misalignment and other modeling errors. An INS exploits aiding sensors to compensate for the drift, functioning as a feedback control system. For submerged craft, aiding can be provided by hydroacoustic position reference (HPR) systems, Doppler velocity log (DVL) and pressure sensors. For aerial vehicles, global navigation satellite systems (GNSS) and altimeters are frequently used as INS aiding. For marine surface craft, both HPR and GNSS based reference systems together with other local position reference systems are used to combat this drift.

For marine surface craft, sole usage of conventional GNSS aiding is not optimal due to the low precision of the vertical position measurement compared to the horizontal counterparts. In heave estimation, the low-quality GNSS signal is usually not applied. For instance, Godhavn (1998) utilized an IMU and a bandpass filter motivated by that the average heave position of a marine surface craft is zero. The technique of Godhavn (1998) was recently modified by Richter et al. (2014) to compensate for amplitude and phase errors by using additional adaptive filters.

Motivated by the fact that the vertical motion of a marine surface craft is zero on average, relative the mean sea surface, Bryne et al. (2014) proposed a virtual vertical reference (VVR) as an alternative to the vertical GNSS measurement by introducing a virtual aiding technique for strapdown INS aided by GNSS. This is done by exploiting the previous GNSS/INS integration framework of Grip et al. (2013) and customizing it for marine surface craft utilization such that the VVR could be applied. An alternative to the VVR concept, with potentially higher precision, is real-time kinematic (RTK) GNSS as presented in Godhavn (2000). However, RTK is limited by the baseline from the receiver to the base station which can be the main limiting factor at sea.

The utilization of INS in marine and offshore applications is likely to increase due to technological advances and price reduction of high-quality IMUs based on micro-electro-mechanical system (MEMS) technology. This paper takes on a simulation study to show how incorporation of a VVR concept, employed as vertical aid, improves the heave estimation performance of strapdown INS for marine surface craft compared to conventional uncoupled and loosely coupled integrated navigation systems employing GNSS and differential GNSS (dGNSS) as reference. Due to kinematic couplings, improvements are also excepted in the attitude estimates. Even though virtual measurements

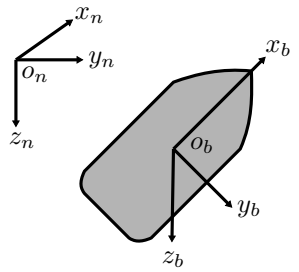

Fig. 1. Definitions of the BODY {b} and NED {n} reference frames.

related to the estimation and navigation literature are well established, e.g. Simon (2009), Ch. 7.5 and Groves (2013), Ch.15.4, to the authors knowledge, our works are the first to propose the VVR aiding solution presented below.

2. PRELIMINARIES

This section presents the modeling needed to represent a strapdown INS with the respective transient GNSS error models. The required augmentation of the strapdown INS model to incorporate the VVR as vertical aiding, applied to marine surface craft, is also introduced.

2.1 Reference Frames

This paper employs two reference frames; The North-East-Down (NED) and BODY reference frames, denoted $\{n\}$ and $\{b\}$, respectively (see Fig. 1). NED is a local Earth-fixed frame, here assumed non-rotating, while the BODY frame is fixed to the vessel. The origin of {b} is located at the nominal center of gravity of the vessel. The x-axis is directed from aft to fore, the y-axis is directed to starboard and the z-axis points downwards.

2.2 Kinematic Strapdown Equations

A strapdown INS is represented using the NED position, $\boldsymbol{p}^n \in \mathbb{R}^3$ and velocity, $\boldsymbol{v}^n \in \mathbb{R}^3$ according to:

$$\dot{\boldsymbol{p}}^n = \boldsymbol{v}^n \tag{1}$$

$$\dot{\boldsymbol{v}}^n = \boldsymbol{R}_b^n \boldsymbol{f}^b + \boldsymbol{g}^n \tag{2}$$

Here, $\boldsymbol{R}_b^n \in SO(3)$ is the rotation matrix from BODY to NED, $\boldsymbol{g}^n \in \mathbb{R}^3$ is the local gravity vector and $\boldsymbol{f}^b = (\boldsymbol{R}_b^n)^\intercal(\dot{\boldsymbol{v}}^n - \boldsymbol{g}^n) \in \mathbb{R}^3$ is the specific force decomposed in {b}. The attitude, $\boldsymbol{R}_b^n$, can by given as a nine parameter rotation matrix (e.g. direction cosine matrix) or by using a unit quaternion, $\boldsymbol{q}_b^n$ such that $\boldsymbol{R}_b^n = \boldsymbol{R}(\boldsymbol{q}_b^n)$. The unit quaternion is defined as $\boldsymbol{q}_b^n =: [s,\, \boldsymbol{r}^\intercal]^\intercal$ where $s \in \mathbb{R}^1$ is the real part, while $\boldsymbol{r} \in \mathbb{R}^3$ constitutes the vector part of the quaternion. Depending of the representation, the attitude either evolves as:

$$\dot{\boldsymbol{R}}_b^n = \boldsymbol{R}_b^n \boldsymbol{S}(\boldsymbol{\omega}_{b/n}^b) \tag{3}$$

or according to

$$\dot{\boldsymbol{q}}_b^n = \boldsymbol{T}(\boldsymbol{q}_b^n)\boldsymbol{\omega}_{b/n}^b \tag{4}$$

where $\boldsymbol{\omega}_{b/n}^b \in \mathbb{R}^3$ is the angular velocity decomposed in {b}. Furthermore, the angular velocity transformation can be given by $\boldsymbol{T}(\boldsymbol{q}_b^n) = [-\boldsymbol{r},\, s\boldsymbol{I}_3 + \boldsymbol{S}^\intercal(\boldsymbol{r})]^\intercal$ as in Fossen (2011), Ch. 2. $\boldsymbol{I}_3 \in \mathbb{R}^3$ is the identity matrix. In addition, $\boldsymbol{S}(\cdot)$ is the skew-symmetric matrix such that $\boldsymbol{v}_1 \times \boldsymbol{v}_2 = \boldsymbol{S}(\boldsymbol{v}_1)\boldsymbol{v}_2$ for two given vectors $\boldsymbol{v}_1, \boldsymbol{v}_2 \in \mathbb{R}^3$. The quaternion update of (4) is equivalent to $\dot{\boldsymbol{q}}_b^n = \boldsymbol{q}_b^n \otimes [0, (\boldsymbol{\omega}_{b/n}^b)^\intercal]^\intercal$. where $\otimes$ denotes the Hamiltonian quaternion product.

In order to incorporate our VVR concept in the observer design, the kinematics of (1)–(4) is extended with the auxiliary variable p_I^n. The augmentation is motivated by the fact that the mean vertical position of the vessel is assumed zero over time since the wave-induced motion of the craft in heave oscillates about the mean sea surface. From Godhavn (1998) we can write:

$$p_I^n = \lim_{T\to\infty} \frac{1}{T} \int_0^T p_z^n(t)\mathrm{d}t = 0 \tag{5}$$

Further on, from (5) we augment (1) by introducing p_I^n as a state with

$$\dot{p}_I^n = p_z^n, \tag{6}$$

by integrating the vertical (down) position associated with the heave motion. In addition, the strapdown equations can be extend further to take into account a three-axis gyro bias, $\boldsymbol{b}_g^b \in \mathbb{R}^3$, here assumed constant, with:

$$\dot{\boldsymbol{b}}_g^b = \boldsymbol{0}. \tag{7}$$

2.3 Sensor Configuration

The loosely coupled INS integration configuration, for fusing IMU, compass, GNSS and VVR measurements, was chosen as:

(1) Position measurements from a GNSS receiver given in the $\{n\}$ frame, $\boldsymbol{p}_{\text{GNSS}}^n = \boldsymbol{p}^n$.
(2) VVR: $p_I^n = 0$, for all $t \geq 0$.
(3) Angular velocity measurements in the $\{b\}$ frame from a three-axis rate gyro with biases: $\boldsymbol{\omega}_{\text{IMU}}^b = \boldsymbol{\omega}_{b/n}^b + \boldsymbol{b}_g^b$. The biases, $\boldsymbol{b}_g^b$, are assumed constant with respect to the system dynamics of (7).
(4) Specific force measurements in the $\{b\}$ frame: $\boldsymbol{f}_{\text{IMU}}^b = \boldsymbol{f}^b$. Accelerometer biases are assumed to be compensated at system start up or by online estimation, utilizing e.g. Grip et al. (2012), Sec. VI.
(5) Heading measurements from a compass, $\psi_c = \psi$.

It should be mentioned that the VVR zero-reading should not be considered as a perfect measurement even though it is free of noise. This is due to the fact that the integrated heave position is only zero on average. Hence, the VVR is not applicable as an equality constraint in constrained estimation frameworks such as Simon (2009), Ch.7.5.

2.4 Transient GNSS Error Modeling

The transient GNSS error, $\boldsymbol{z} = [z_n,\, z_e,\, z_d]^\intercal$, can for simulation purposes be modeled as a three-dimensional, first-order, discrete-time Gauss-Markov process

$$\boldsymbol{z}(k+1) = \boldsymbol{\Phi}_{\text{GNSS}}\, \boldsymbol{z}(k) + \boldsymbol{w}_{GNSS}(k), \tag{8}$$

where $\boldsymbol{\Phi}_{\text{GNSS}} = \boldsymbol{I}_3 \cdot \exp\left(-\frac{1}{T} \cdot T_s\right)$ obtained from Rankin (1994), where k denotes the time index, while $\boldsymbol{w}_{GNSS}(k)$ is the driving Gaussian white noise of (8). Furthermore, T is the correlation time constant and T_s is the sampling time of the modeled GNSS receiver. The resulting position measurements provided by the receiver in {n} can then be given as:

$$\boldsymbol{p}_{\text{GNSS}}^n(k) = \boldsymbol{p}^n(k) + \boldsymbol{z}(k) + \boldsymbol{\epsilon}(k). \tag{9}$$

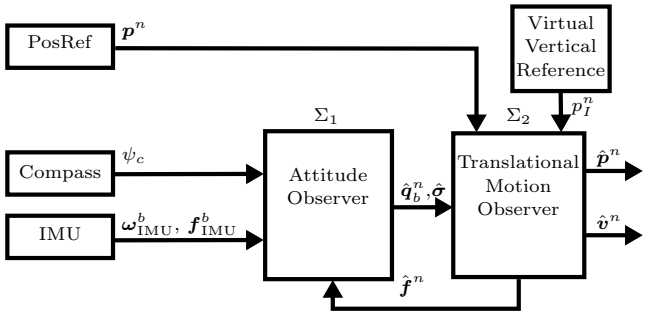

Fig. 2. Feedback-interconnected observer structure.

where $\boldsymbol{\epsilon}(k)$ is residual Gaussian white noise. This error model is used only for simulations and is not exploited by the observer.

3. NONLINEAR OBSERVER DESIGN

The nonlinear observer design consists of two feedback-interconnected observers, estimating attitude and translational motion, denoted Σ_1 and Σ_2, respectively. The observer structure is illustrated in Fig. 2.

3.1 Nonlinear attitude observer

The nonlinear attitude observer, Σ_1, by Grip et al. (2013), based upon Grip et al. (2012) and Mahony et al. (2008), is given by

$$\Sigma_1 : \begin{cases} \dot{\hat{\boldsymbol{q}}}_b^n = \boldsymbol{T}(\hat{\boldsymbol{q}}_b^n)(\boldsymbol{\omega}_{b/n,\text{IMU}}^b - \hat{\boldsymbol{b}}_g^b + \hat{\boldsymbol{\sigma}}) & \text{(10a)} \\ \dot{\hat{\boldsymbol{b}}}_g^b = \text{Proj}(\hat{\boldsymbol{b}}_g^b, -k_I \hat{\boldsymbol{\sigma}}). & \text{(10b)} \end{cases}$$

with the injection term,

$$\hat{\boldsymbol{\sigma}} = k_1 \boldsymbol{c}^b \times \boldsymbol{R}(\hat{\boldsymbol{q}}_b^n)^\intercal \boldsymbol{c}^n + k_2 \boldsymbol{f}_{\text{IMU}}^b \times \boldsymbol{R}(\hat{\boldsymbol{q}}_b^n)^\intercal \hat{\boldsymbol{f}}^n \quad (11)$$

where $k_I > 0$ in (10b) and the gains in (11) satisfies $k_1 \geq k_P$ and $k_2 \geq k_P$ for some $k_P > 0$. The vector measurement based on ψ_c, from the compass, is defined as $\boldsymbol{c}^b := [\cos(\psi_c), -\sin(\psi_c), 0]^\intercal$ whereas the reference vector is defined as $\boldsymbol{c}^n := [1, 0, 0]^\intercal$. $\boldsymbol{f}_{\text{IMU}}^b$ is measured specific force provided by the accelerometer, while $\hat{\boldsymbol{f}}^n$ is provided by Σ_2 and is the estimated specific force in the $\{\text{n}\}$ frame. $\text{Proj}(\cdot,\cdot)$ denotes the parameter projection, from Krstić et al. (1995), App. E, such that the gyro bias estimate is confined to a compact set, $\|\hat{\boldsymbol{b}}_g^b\| \leq M_g$, as with the previous results presented by Grip et al. (2013).

3.2 Translational motion observer

The translational motion observer (TMO) Σ_2 is a time-invariant version of Bryne et al. (2014) with the model augmentation of (6) given by:

$$\Sigma_2 : \begin{cases} \dot{\hat{p}}_I^n = \hat{p}_z^n + \theta_{hg} K_{pIpI} \tilde{p}_I & \text{(12a)} \\ \dot{\hat{\boldsymbol{p}}}^n = \hat{\boldsymbol{v}}^n + \theta_{hg}^2 \begin{bmatrix} \boldsymbol{0}_{2\times 1} \\ K_{ppI} \end{bmatrix} \tilde{p}_I + \theta_{hg} \boldsymbol{K}_{pp} \boldsymbol{C}_{\text{p}} \tilde{\boldsymbol{p}} & \text{(12b)} \\ \dot{\hat{\boldsymbol{v}}}^n = \hat{\boldsymbol{f}}^n + \boldsymbol{g}^n + \theta_{hg}^3 \begin{bmatrix} \boldsymbol{0}_{2\times 1} \\ K_{vpI} \end{bmatrix} \tilde{p}_I \\ \qquad + \theta_{hg}^2 \boldsymbol{K}_{vp} \boldsymbol{C}_{\text{p}} \tilde{\boldsymbol{p}} & \text{(12c)} \\ \dot{\boldsymbol{\xi}} = -\boldsymbol{R}(\hat{\boldsymbol{q}}_b^n) \boldsymbol{S}(\hat{\boldsymbol{\sigma}}) \boldsymbol{f}_{\text{IMU}}^b + \theta_{hg}^4 \begin{bmatrix} \boldsymbol{0}_{2\times 1} \\ K_{\xi pI} \end{bmatrix} \tilde{p}_I \\ \qquad + \theta_{hg}^3 \boldsymbol{K}_{\xi p} \boldsymbol{C}_{\text{p}} \tilde{\boldsymbol{p}} & \text{(12d)} \\ \hat{\boldsymbol{f}}^n = \boldsymbol{R}(\hat{\boldsymbol{q}}_b^n) \boldsymbol{f}_{\text{IMU}}^b + \boldsymbol{\xi}, & \text{(12e)} \end{cases}$$

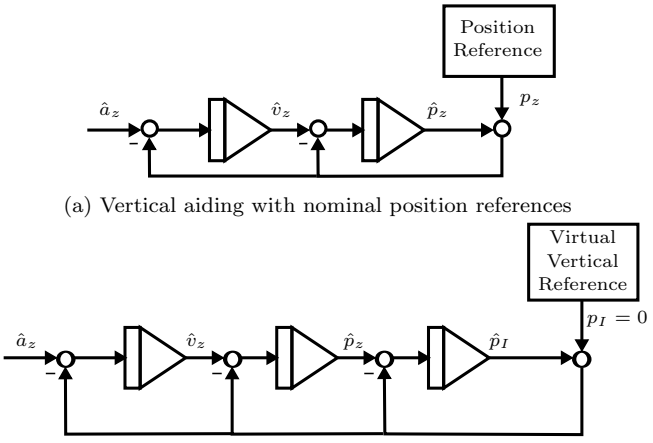

(a) Vertical aiding with nominal position references

(b) Vertical aiding with the VVR concept

Fig. 3. Illustration: Block diagram of nominal aiding from a position reference vs. the VVR aiding concept. The feedback gains are not included. The z-subscript refers to the vertical z-axis of the translational motion

where $\tilde{p}_I = p_I^n - \hat{p}_I^n$, $\tilde{\boldsymbol{p}} = \boldsymbol{p}_{\text{GNSS}}^n - \hat{\boldsymbol{p}}^n$. $K_{[\cdot]p_I}$ and $\boldsymbol{K}_{[\cdot]p}$ are the respective gains, while $\theta_{hg} \geq 1$ is a high-gain tuning parameter used to guarantee stability. $\boldsymbol{C}_{\text{p}} = \text{diag}\,(1, 1, 0)$ is a matrix applied to omit the vertical GNSS measurement component in the observer design. Since the VVR provides $p_I^n = 0$ for all $t \geq 0$, the vertical estimates of Σ_2 are self contained regardless of GNSS precision and accuracy or GNSS position fix.

In order to illustrate the effect of the VVR measurement compared to using vertical GNSS and dGNSS measurements, another TMO is also presented. This TMO is denoted $\Sigma_{2,\text{nom}}$ and refers to the nominal TMO of Grip et al. (2013), without velocity and VVR measurements, solely utilizing the vertical GNSS measurement to stabilize the vertical axes. $\Sigma_{2,\text{nom}}$ is given as:

$$\Sigma_{2,\text{nom}} : \begin{cases} \dot{\hat{\boldsymbol{p}}}^n = \hat{\boldsymbol{v}}^n + \theta_{hg} \boldsymbol{K}_{pp} \tilde{\boldsymbol{p}} & \text{(13a)} \\ \dot{\hat{\boldsymbol{v}}}^n = \hat{\boldsymbol{f}}^n + \boldsymbol{g}^n + \theta_{hg}^2 \boldsymbol{K}_{vp} \tilde{\boldsymbol{p}} & \text{(13b)} \\ \dot{\boldsymbol{\xi}} = -\boldsymbol{R}(\hat{\boldsymbol{q}}_b^n) \boldsymbol{S}(\hat{\boldsymbol{\sigma}}) \boldsymbol{f}_{\text{IMU}}^b + \theta_{hg}^3 \boldsymbol{K}_{\xi p} \tilde{\boldsymbol{p}} & \text{(13c)} \\ \hat{\boldsymbol{f}}^n = \boldsymbol{R}(\hat{\boldsymbol{q}}_b^n) \boldsymbol{f}_{\text{IMU}}^b + \boldsymbol{\xi}. & \text{(13d)} \end{cases}$$

Also this observer is feedback interconnected with Σ_1, similar to Fig. 2 without aiding from the VVR. The difference in how the two TMOs performs the vertical aiding is shown in Fig. 3, where Fig. 3a illustrates the nominal GNSS aiding, while Fig. 3b shows how the virtual aiding technique can be incorporated into the INS's vertical channel. The error dynamics of $\Sigma_1 - \Sigma_{2,\text{nom}}$ and $\Sigma_1 - \Sigma_2$ were proven to be uniformly semiglobal exponential stable (USGES) in Grip et al. (2013) and Bryne et al. (2014), respectively.

4. CASE STUDY

This section will present the result of utilizing the VVR as vertical INS aiding. First we will present results of the transient precision of vertical GNSS and dGNSS measurements before we show how Σ_2 potentially increases the estimation accuracy compared using $\Sigma_{2,\text{nom}}$ as TMO.

Table 1. GNSS error-model parameters.

	Std. Dev. $\boldsymbol{w}$ [m]	Corr. time T [s]	T_s [Hz]
North	0.21	1100	1.0
East	0.21	1100	1.0
Down	0.40	1100	1.0

4.1 Simulation Details

The sensor measurements were generated using the Marine Systems Simulator (2010) simulating a offshore supply vessel employing a DP system. The vessel's wave-induced motions were generated by exposing the vessel to wave forces and moments generated with the JONSWAP wave spectra. The significant wave height and peak frequency were chosen as, $H_s = 7$ [m] and $\omega_0 = 0.8$ [rad/s], respectively. The IMU and the respective observers where simulated at 100 Hz. Gaussian white noise was added to IMU measurements. The chosen heading and position measurements were simulated at 10 Hz and 1 Hz, respectively. Hence, the GNSS correction of the TMOs was carried out at 1 Hz using the corrector-predictor implementation of Fossen (2011), Ch. 11.3.4. The compass error was simulated as a Gauss-Markov process. The same model was chosen to generate the GNSS errors. Modeling details are presented next.

4.2 GNSS Transient Error

We have chosen to simulate two types of GNSS receivers. One standalone receiver and one with differential correction. The parameters of (8) for the standalone receiver is based on Beard and McLain (2012), Tab. 7.2, p. 139 and presented in Table 1. An example of the transient GNSS-error realization is shown in Fig. 4.

The dGNSS receiver correlation time is based on the results of Rankin (1994) and Mohleji and Wang (2010) where the former suggests a correlation time of 10 minutes for a simulated dGPS receiver, while the latter suggest a correlation time in the range of $4-8$ minutes. Since the results presented in Mohleji and Wang (2010) are recent and hence more up to date with respect to hardware and software solutions, this recommendation constituted the basis for our dGNSS realization of (8). The driving noise was selected such that the root mean square (RMS) errors of $\boldsymbol{z}(k)$ over a large time horizon was between 1 and 2 meters in North and East, while the vertical component was in the range of $2-4$ meters. The chosen model parameters of the dGNSS receiver are presented in Table 2.

Realizations of (8) for GNSS and dGNSS transient errors are shown in Figs. 4–5, respectively. The RMS errors of these realizations are further given in Table 3.

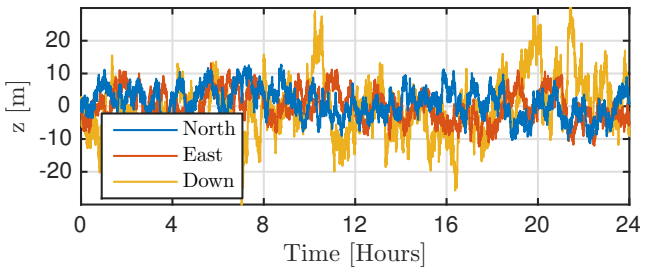

Fig. 4. Example of GNSS error realization

Table 2. dGNSS error-model parameters.

	Std. Dev. $\boldsymbol{w}$ [m]	Corr. time T [s]	T_s [Hz]
North	0.1	480	1.0
East	0.1	480	1.0
Down	0.2	480	1.0

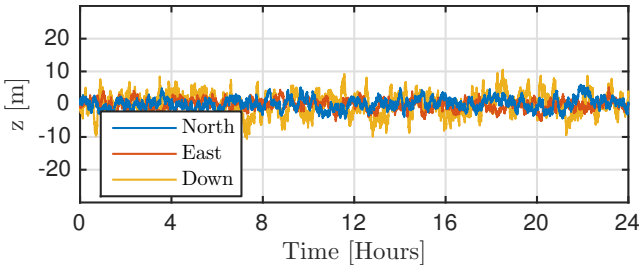

Fig. 5. Example of dGNSS error realization

Table 3. GNSS and dGNSS RMS errors of Figs. 4–5

Measurement Component	**GNSS RMS error [m]**	**dGNSS RMS error [m]**
North	4.4963	1.7300
East	4.8527	1.4609
Down	9.1083	3.2377

4.3 Tuning

The gains associated with the horizontal axes were chosen equal for both observers: $\boldsymbol{K}_{pp_{xy}} = 0.4190 \cdot \boldsymbol{I}_2$, $\boldsymbol{K}_{vp_{xy}} = 0.0878 \cdot \boldsymbol{I}_2$ and $\boldsymbol{K}_{\xi p_{xy}} = 0.0091 \cdot \boldsymbol{I}_2$, while the gains associated with the vertical axes of $\Sigma_{2,\text{nom}}$ and Σ_2 are given in Table 4 such that $\boldsymbol{K}_{pp} = \text{diag}(\boldsymbol{K}_{pp,xy}, K_{p_zp_z})$, $\boldsymbol{K}_{vp} = \text{diag}(\boldsymbol{K}_{vp,xy}, K_{v_zp_z})$ and $\boldsymbol{K}_{\xi p} = \text{diag}(\boldsymbol{K}_{\xi p,xy}, K_{\xi_zp_z})$. The gains associated with the same states were chosen similar for both observer such that the comparison would be relevant.

$\theta_{hg} = 1$ was chosen for both $\Sigma_{2,\text{nom}}$ and Σ_2. Regarding the attitude observer, the measurement/references vector pair were normalized and given equal weights using $k_1 = k_2 = 0.55$, while k_I was chosen $k_I = 0.01$.

4.4 Simulation Results

Heave accuracy: The respective heave estimates obtained, from applying the three simulated vertical position references, are shown in Figs. 6–8. The heave estimate obtained with aiding from the simulated standalone GNSS receiver is shown in Fig. 6 together with the actual heave motion of the ship. Fig. 7 shows the transient performance of the heave estimate obtained from utilizing the simulated dGNSS receiver. An improvement in heave estimation performance, when compared to Fig. 6, is observed. The heave estimate, using the VVR measurement as vertical aid is shown in Fig. 8. One can clearly observe the increase in heave estimation accuracy by utilizing Σ_2 as TMO with the VVR aiding concept. This is also observed in Fig. 9, comparing the respective heave estimation errors. Fig. 9 show the steady state estimation error utilizing the three

Table 4. Vertical Gains Tuning of Σ_2

$\boldsymbol{\Sigma_{2,\text{nom}}}$		$\boldsymbol{\Sigma_2}$	
-	-	$K_{p_Ip_I}$	0.4655
$K_{p_zp_z}$	0.1083	$K_{p_zp_I}$	0.1083
$K_{v_zp_z}$	0.0148	$K_{v_zp_I}$	0.0148
$K_{\xi_zp_z}$	0.0010	$K_{\xi_zp_I}$	0.0010

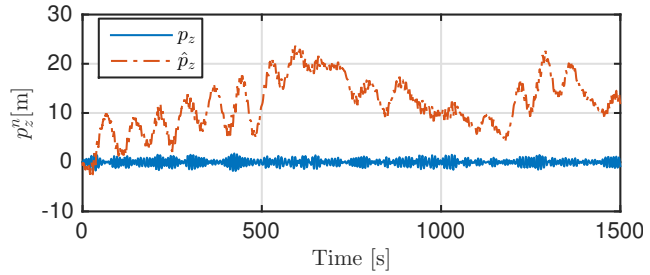

Fig. 6. Heave estimate using a standalone GNSS receiver as vertical position reference

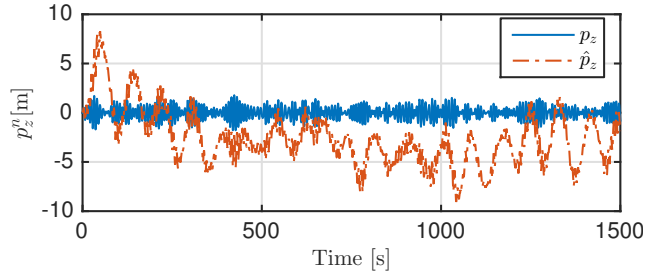

Fig. 7. Heave estimate using a dGNSS receiver as vertical position reference

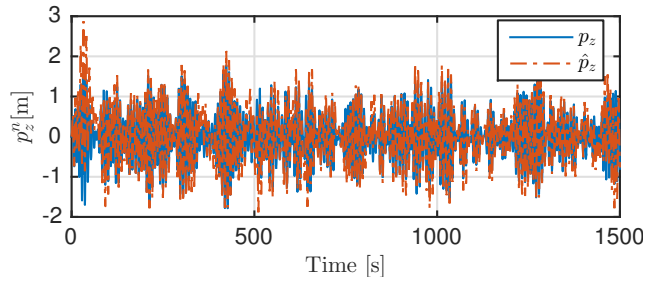

Fig. 8. Heave estimate with state-space augmentation and using the VVR as vertical position reference

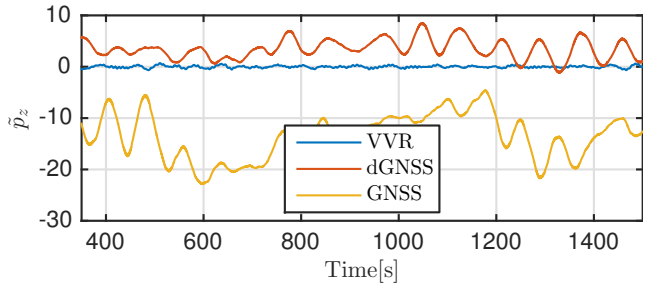

Fig. 9. Steady state heave estimation error.

vertical position references as INS aid. It is evident that the VVR aiding results in the highest heave estimation accuracy and that standalone GNSS aiding yields the lowest. This is also confirmed by Table 5 where the heave estimation RMS error together with the mean square errors (MSE) and the cumulative estimation error (CEE) at time 1500 seconds are presented. The MSE is defined as:

$$MSE := \frac{1}{N}\sum_{k=1}^{N}\left(x(k) - \hat{x}(k)\right)^2, \tag{14}$$

while the CEE is defined as

$$CEE := \sum_{k=1}^{N}\left|x(k) - \hat{x}(k)\right|, \tag{15}$$

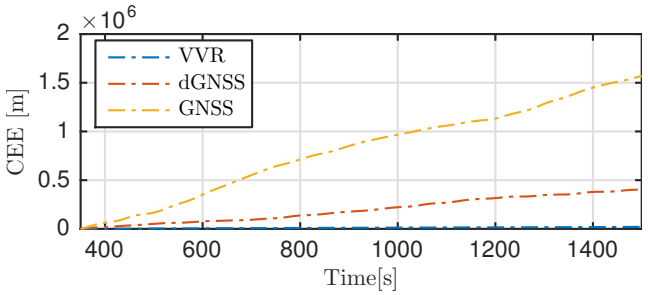

Fig. 10. Heave CEE starting at time = 350 s

where $x = p_z$ when evaluating the heave estimation error. Fig. 10 shows how the heave CEEs evolves over time. The heave CEE is significantly less than compared to the CEE obtained with a GNSS based vertical INS aiding. The statistics presented in Table 5 are calculated in steady state, i.e after the attitude estimate had converged, between 350 and 1500 seconds of simulation.

Table 5. Heave: Estimation error statistics

Vertical Aiding	**RMS [m]**	**MSE [m^2]**	**CEE [m] (at time 1500 s)**
VVR	0.1889	0.0357	20753.80
dGNSS	1.5063	2.2691	403155.62
GNSS	7.3705	60.1101	1569456.65

Additional comments related to the estimation performance are presented in Section 4.5.

Roll and pitch accuracies: Since the observers Σ_1–$\Sigma_{2,\text{nom}}$ and Σ_1–Σ_2 are feedback interconnected, the accuracy of the translational motion estimates will effect the attitude estimates through the feedback. To show the relationship between the vertical translational motion estimates and the roll and pitch estimates, we start with the term

$$k_2 \boldsymbol{f}^b_{\text{IMU}} \times \boldsymbol{R}(\hat{\boldsymbol{q}}^n_b)^\intercal \hat{\boldsymbol{f}}^n$$

from the attitude observer injection term, $\hat{\boldsymbol{\sigma}}$, given in (11). Moreover, we express the transposed estimated attitude term, $\boldsymbol{R}(\hat{\boldsymbol{q}}^n_b)^\intercal$, in terms of Euler angles with

$$\begin{aligned}\boldsymbol{R}(\hat{\boldsymbol{q}}^n_b)^\intercal &= (\hat{\boldsymbol{R}}^n_b)^\intercal \\ &= \begin{bmatrix} R_{11} & R_{12} & R_{13} \\ R_{21} & R_{22} & R_{23} \\ -\mathrm{s}\hat{\theta} & \mathrm{c}\hat{\theta}\mathrm{s}\hat{\phi} & \mathrm{c}\hat{\theta}\mathrm{c}\hat{\phi} \end{bmatrix}^\intercal = \begin{bmatrix} R_{11} & R_{21} & -\mathrm{s}\hat{\theta} \\ R_{12} & R_{22} & \mathrm{c}\hat{\theta}\mathrm{s}\hat{\phi} \\ R_{13} & R_{23} & \mathrm{c}\hat{\theta}\mathrm{c}\hat{\phi} \end{bmatrix}\end{aligned} \tag{16}$$

with $\mathrm{s}\cdot = \sin(\cdot)$ and $\mathrm{c}\cdot = \cos(\cdot)$, where R_{ij}, $i = [1,2], j = [1,2,3]$ is found in Fossen (2011), eq. (2.18), p. 22. For marine surface craft, the mapping from the unit quaternion to Euler angles is always well defined since a pitch angle of $\pm 90°$ represent an infeasible attitude for surface craft. By postmultiplying $\hat{\boldsymbol{R}}^b_n$ with the vertical component of $\hat{\boldsymbol{f}}^n$ results in:

$$\hat{\boldsymbol{R}}^b_n \cdot \begin{bmatrix} 0 \\ 0 \\ \hat{f}^n_z \end{bmatrix} = \begin{bmatrix} -\mathrm{s}\hat{\theta} \\ \mathrm{c}\hat{\theta}\mathrm{s}\hat{\phi} \\ \mathrm{c}\hat{\theta}\mathrm{c}\hat{\phi} \end{bmatrix} \hat{f}^n_z. \tag{17}$$

Hence, it is evident from (17) that the roll and pitch estimates are strongly coupled with the vertical component of $\hat{\boldsymbol{f}}^n$ from the TMO. Furthermore, one can also argue that if the precision of the vertical reference measurement, which updates the specific force estimate, increases, potentially

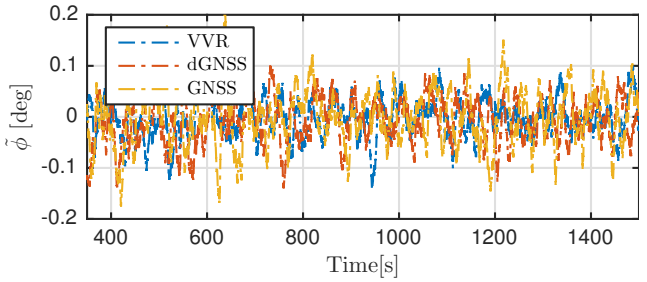

Fig. 11. Steady state roll estimation error

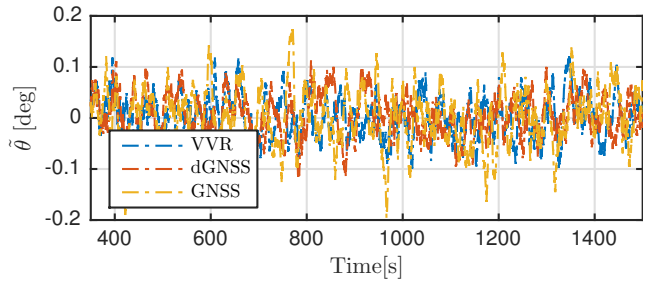

Fig. 12. Steady state pitch estimation error

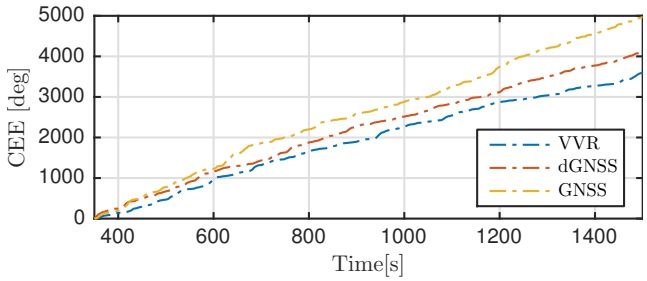

Fig. 13. Roll CCE starting at time 350 s

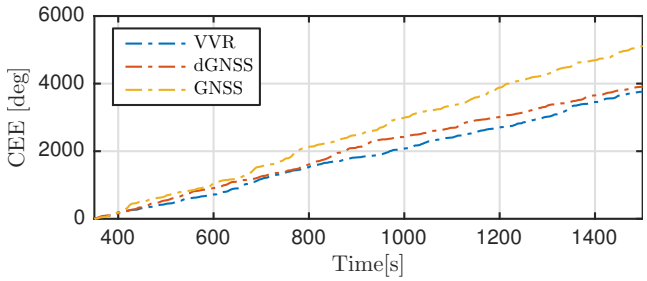

Fig. 14. Pitch CEE starting at time 350 s

the roll and pitch estimate accuracy is also increased. This effect can be observed in Figs. 11–12 where the conventional GNSS aiding results in the lowest roll and pitch estimate accuracy compared to those obtained using the VVR or dGNSS as vertical aid. The statistics of the steady state roll and pitch estimation errors are given in Tables 6–7, respectively. The highest accuracy is obtained with the VVR and dGNSS aiding. Figs. 13–14, presenting the evolution of CEEs for the respective roll and pitch estimates, show that the CEEs are significantly less over time when utilizing VVR and dGNSS, as vertical aiding measurement, than compared to the respective counterparts when utilizing a standalone GNSS receiver.

Table 6. Roll: Estimation error statistics.

Vertical Aiding	**RMS error[deg]**	**MSE [deg^2]**	**CEE [deg] (at time 1500 s)**
VVR	0.0459	0.0021	3591.86
dGNSS	0.0400	0.0016	4089.26
GNSS	0.0597	0.0036	4965.17

Table 7. Pitch: Estimation error statistics.

Vertical Aiding	**RMS error [deg]**	**MSE [deg^2]**	**CEE [deg] (at time 1500 s)**
VVR	0.0422	0.0018	3762.17
dGNSS	0.0412	0.0017	3906.10
GNSS	0.0577	0.0033	5117.92

4.5 Additional Comments

It should be mentioned that the heave estimation precision of Fig. 8 and metrics associated with the VVR in Table 5 is sea state dependent. For sea states with low peak frequency, ω_0, of the wave spectra, the precision of the heave estimate with the VVR measurement update will decrease if the gains of Σ_2 is not modified accordingly. This is due to the low-pass characteristics of the observer combined with low frequency estimated acceleration input, $\hat{\boldsymbol{a}}^n = \hat{\boldsymbol{f}}^n + \boldsymbol{g}^n$, together will inflict phase error on the heave estimates.

The accuracy of marine GNSS receiver's height measurement can be increased by applying a model representing an approximation of the craft's vertical movements. This model is then utilized by the receiver's Kalman filter. This can for instance be a PV model:

$$\dot{p}_z^n = v_z^n \tag{18}$$
$$\dot{v}_z^n = w \tag{19}$$

or a Gauss-Markov process model

$$\dot{p}_z = -\frac{1}{T} p_z + w \tag{20}$$

where w is some Gaussian white noise. However, this strategy is not without downsides. The noise power of w has to be modified to take in account changes in the wave height to yield optimal performance. Moreover, modifying off-the-shelf receivers are not necessarily applicable.

Regarding tightly coupled integration schemes where pseudoranges are the observables, the VVR concept has the potential to increase the GNSS accuracy also in the horizontal plane with similar effect as differential correction. This is due to the heave estimates from the INS are fed back to the pseudorange resolver. By emphasizing that VVR measurement, in general, is more accurate than the pseudoranges (user equivalent range error (URE) RMS is typically $\sim$ 6 [m], Misra and Enge (2011), Tab. 5.3, p. 179, for single-frequency receivers), common-mode errors effecting the position both in horizontal and vertical axes, may be interpreted as a receiver-clock error. The latter should always be estimated with tightly coupled GNSS/INS integration if four or more pseudorange measurements are available. In addition, tightly coupled integration will always have some aiding in the vertical axis from the GNSS pseudoranges even though the VVR is the primary vertical aiding. This has the potential to combat some of the phase errors induced by high sea states. For details related to GNSS/INS integration Titterton and

Weston (2004), Grewal et al. (2013) or Groves (2013) can be advised.

5. CONCLUSIONS

A concept for more accurate aiding of inertial navigation systems (INS) for marine surface craft has been presented. The main idea is to use the mean surface level of the ocean as a virtual measurement since this will be zero on average. A nonlinear interconnected observer for estimation of the attitude and translational motion have been reconstructed to utilize the vertical virtual reference (VVR) measurement together with GNSS horizontal position measurements. Exponential stability of the observer estimation errors are guaranteed by previously published results.

Computer simulations of offshore vessels verify that strapdown inertial navigation systems aided by a VVR improves the accuracy of the navigation system significantly when compared to conventional loosely coupled GNSS aiding techniques. The heave, roll and pitch estimates are more accurate with VVR aiding than obtained with standalone GNSS receiver aiding. The VVR is also a simple concept, being self contained and independent of differential corrections.

ACKNOWLEDGEMENTS

This work has been carried out at the Centre for Autonomous Marine Operations and Systems (AMOS) and supported by the Research Council of Norway and Rolls-Royce Marine through the Centres of Excellence funding scheme and the MAROFF programme. Grant numbers 223254 and 225259, respectively. The Research Council of Norway is acknowledged as the main sponsor of AMOS.

The authors wish to thank Dr. Nadezda Sokolova at the Department of Engineering Cybernetics, Norwegian University of Sciences and Technology and SINTEF ICT, and Dr. Aiden Morrison, SINTEF ICT for valuable discussions on GNSS systems.

REFERENCES

Beard, R.W. and McLain, T.W. (2012). *Small Unmanned Aircraft: Theory and Practice*. Princeton University Press.

Bryne, T.H., Fossen, T.I., and Johansen, T.A. (2014). Nonlinear observer with time-varying gains for inertial navigation aided by satellite reference systems in dynamic positioning. In *IEEE Mediterranean Conference on Control and Automation*, 1353–1360. doi:10.1109/MED.2014.6961564.

Fossen, T.I. (2011). *Handbook of Marine Craft Hydrodynamics and Motion Control*. John Wiley & Sons, Ltd.

Godhavn, J.M. (1998). Adaptive tuning of heave filter in motion sensor. In *OCEANS '98 Conf. Proc.*, volume 1, 174–178. Nice, France. doi:10.1109/OCEANS.1998.725731.

Godhavn, J.M. (2000). High quality heave measurements based on GPS RTK and accelerometer technology. In *OCEANS 2000 MTS/IEEE Conference and Exhibition*, volume 1, 309–314. Providence, RI. doi:10.1109/OCEANS.2000.881277.

Grewal, M., Andrews, A.P., and Bartone, C.G. (2013). *Global navigation satellite systems, inertial navigation, and integration*. John Wiley & Sons, Inc., Hoboken, New Jersey, 3rd edition.

Grip, H.F., Fossen, T.I., Johansen, T.A., and Saberi, A. (2012). Attitude estimation using biased gyro and vector measurements with time-varying reference vectors. *IEEE Trans. Automat. Contr.*, 57(5), 1332—1338. doi:10.1109/TAC.2011.2173415.

Grip, H.F., Fossen, T.I., Johansen, T.A., and Saberi, A. (2013). Nonlinear observer for GNSS-aided inertial navigation with quaternion-based attitude estimation. In *Proc. of the American Contr. Conf.*, 272–279. Washington, DC. doi:10.1109/ACC.2013.6579849.

Groves, P.D. (2013). *Principles of GNSS, Inertial, and Multisensor Integrated Navigation Systems*. Artech House, 2nd edition.

Krstić, M., Kanellakopoulos, I., and Kokotović, P.V. (1995). *Nonlinear and Adaptive Control Design*. Wiley, New York.

Mahony, R., Hamel, T., and Pflimlin, J.M. (2008). Nonlinear complementary filters on the special orthogonal group. *IEEE Trans. Automat. Contr.*, 53(5), 1203–2018. doi:10.1109/TAC.2008.923738.

Misra, P. and Enge, P. (2011). *Global Positioning System: Signals, Measurements, and Performance*. Ganga-Jamuna Press, 2nd, revised edition.

Mohleji, S.C. and Wang, G. (2010). Modeling ADS-B position and velocity errors for airborne merging and spacing in interval management application. `https://www.mitre.org/sites/default/files/pdf/10_3026.pdf`, The MITRE Corporation, 7515 Colshire Drive, McLean VA 22102.

MSS. Marine Systems Simulator (2010). Viewed 01.08.2014, `www.marinecontrol.org`.

Rankin, J. (1994). GPS and differential GPS: An error model for sensor simulation. In *IEEE Position Location and Navigation Symposium*, 260–266. Las Vegas, NV. doi:10.1109/PLANS.1994.303322.

Richter, M., Schneider, K., Walser, D., and Sawodny, O. (2014). Real-time heave motion estimation using adaptive filtering techniques. In *Proc. of the 19th IFAC World Congress*, 10119–10125. Cape Town, South Africa. doi:10.3182/20140824-6-ZA-1003.00111.

Simon, D. (2009). *Optimal state estimation: Kalman, H_∞, and nonlinear approaches*. John Wiley & Sons.

Titterton, D.H. and Weston, J.L. (2004). *Strapdown inertial navigation technology*. Institution of Electrical Engineers and American Institute of Aeronautics and Astronautics, 2nd edition.